Supporting Information

Wang and Wolynes 10.1073/pnas.1112034108

SI Text

Numerical Method. We performed dynamical Monte Carlo simulations on the model cytoskeleton (1, 2) to compare with the analytical predictions. In these simulations, we generated initially a three-dimensional random lattice of volumeless nodes (mimicking the cross-linking proteins) and connected the nearest-neighbor nodes (defined by the first shell of the radial distribution function) with nonlinear elastic bonds (mimicking the filamentous proteins) at a given probability P_c, which characterizes the network connectivity. Thermal steps obey Brownian dynamics, whereas chemical moves follow the stochastic process described by the model kicking statistics (Eq. **2** in the main text). We represent the nodes by identical spheres and hide the filaments. To visualize the spontaneous flow (Movies S3–S7), we label a randomly chosen node and its neighbors with bright colors (cyan for the central node and gold for its neighbors), whereas we color the rest of the nodes in red. The directed motion of the labeled nodes then indicates a spontaneous collective motion of the whole lattice in a specific direction. Periodic boundary conditions are adopted. The system size is $N = 256$. For all the following movies, the only varied parameter is the network connectivity P_c; the other parameters remain the same ($L_e = 1.2$, $\beta\gamma = 5$; $s = 1$, $l = 0.25$).

1. Shen T, Wolynes PG (2006) Statistical mechanics of a cat's cradle. *New J Phys* 8:273.
2. Wang S, Shen T, Wolynes PG (2011) The interplay of nonlinearity and architecture in equilibrium cytoskeletal mechanics. *J Chem Phys* 134:014510.

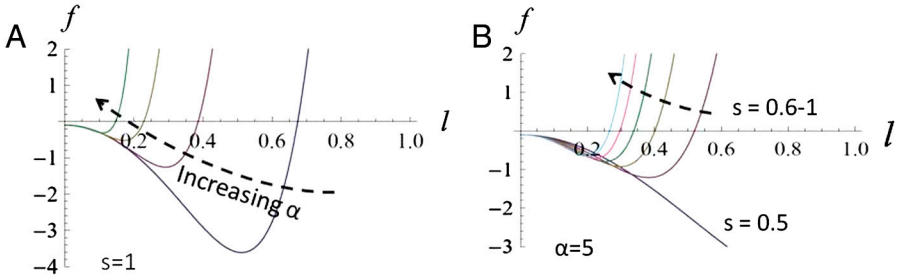

Fig. S1. Dependence of threshold kick step size upon mechanical gradient α and motor susceptibility *s*. We plot $f(l,s;\alpha,\tilde{\alpha})$ given by Eq. **11** in the main text as a function of kick step size *l* for $\kappa = 20$, $D_0 = 0.1$. The crossing point of the *f* curve with the *l* axis locates l_{th}. (*A*) From right to left, $\alpha = 0.1$, 1, 10, and 100; $s = 1$. l_{th} decreases with increasing α value (dashed arrow), indicating that strong mechanical feedback facilitates instability onset. (*B*) For a moderate α value ($\alpha = 5$), no instability onset occurs for $s \leq 0.5$; only after *s* reaches approximately 0.6 does an instability emerge and increasing *s* (dashed arrow) leads to lower l_{th}. Meanwhile, for a given *l*, *f* increases with *s*, suggesting that more susceptible motors drive faster flows.

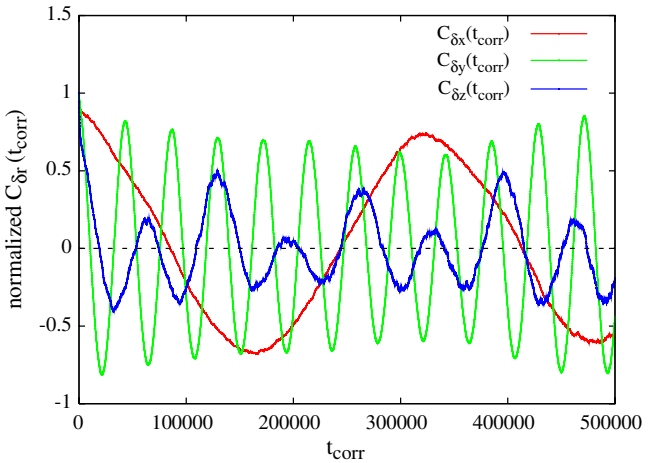

Fig. S2. Statistical characteristics for the flowing state. We plot the ensemble-averaged temporal correlation of displacement fluctuations defined via the correlation function $C_{\delta\vec{r}}(t_{corr}) = \frac{1}{t_f - t_0}\int_{t_0}^{t_f} d\tau [\frac{1}{N}\sum_{i=1}^{N} \delta\vec{r}_i(\tau)][\frac{1}{N}\sum_{j=1}^{N} \delta\vec{r}_j(\tau + t_{corr})]$, where $\delta\vec{r}_i(t) = \vec{r}_i(t) - \langle\vec{r}_i(t)\rangle$ with the bracket indicating an average over a steady-state time window. The integral averages the starting time τ over a wide time range (t_0, t_f). Correlations in three orthogonal spatial directions (*x*, red; *y*, green; *z*, blue) all exhibit periodic oscillations in time (in Monte Carlo units) reflecting the spontaneous and coherent flowing motion across the periodic simulation box. Other correlation measures exhibit consistent oscillatory patterns. Parameters are given by $L_e = 1.2$, $\beta\gamma = 5$, $P_c = 0.5$; $l = 0.25$, $s = 1$.

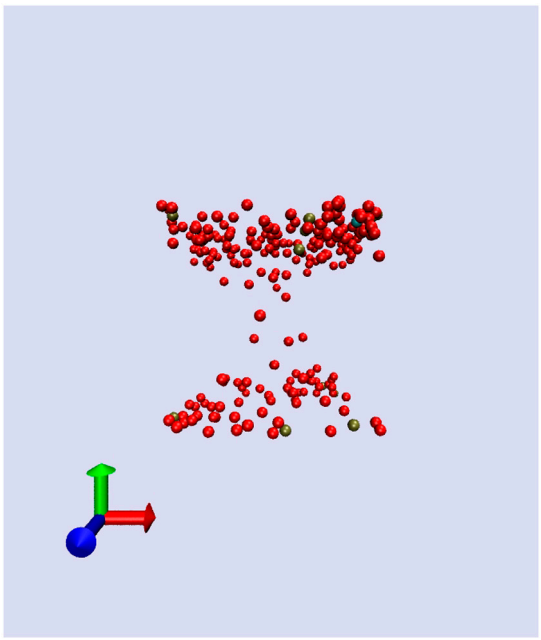

Movie. S1 Development of phase separation. At an intermediate network connectivity ($P_c = 0.3$) tension percolation is efficient, yet local force imbalance becomes significant; under susceptible motor kicking with a considerable step size, dramatic spatial heterogeneity develops and evolves into collapses and oscillations of the nodes in a particular spontaneously chosen direction. Snapshots of the corresponding network structure have been shown in Fig. 3.

Movie S1 (MPG)

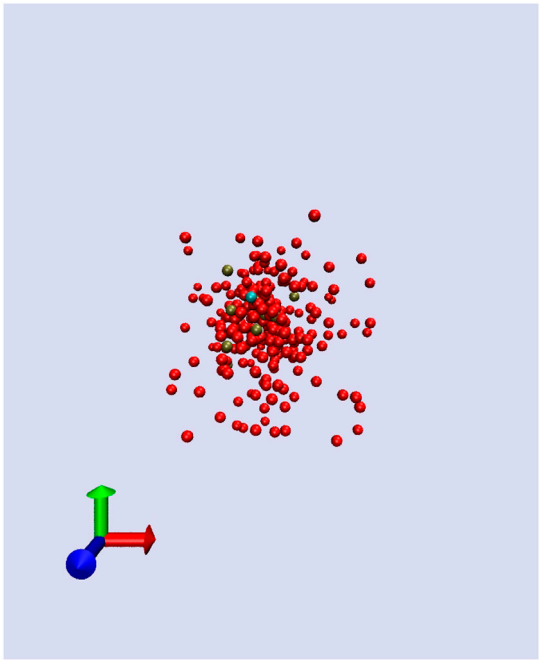

Movie. S2 Failure of force percolation. When the network connectivity becomes too low to achieve global force percolation ($P_c = 0.2$), phase separation still occurs but without a preferred direction of motion.

Movie S2 (MPG)

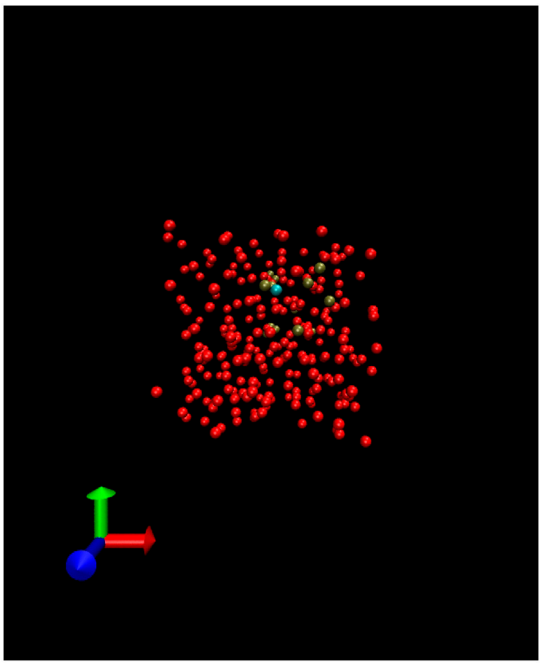

Movie S3 Nonmonotonic dependence of flow initiation and flow speed upon network connectivity. For Movies S3–S7, network connectivity varies with $P_c = 0.4$, 0.5, 0.6, 0.7, and 0.9, respectively. In all the cases, the whole lattice develops spontaneous directed motion and exhibits spatial modulation, indicating modulated flowing states. As P_c increases from 0.4 to 0.6 (Movies S3–S5), flow initiation accelerates and flow speed rises; as P_c further increases to 0.7 (Movie S6) and 0.9 (Movie S7), increasing the number of bond constraints appears to slow down flow initiation and to reduce flow speed. This suggests an optimal network connectivity (and thus optimal localization strength of the nodes) for most efficient flow. Meanwhile, as P_c increases, the nodes exhibit smaller amplitude of vibrations about the moving fiducial lattice and the cage of neighbors (as seen for the labeled nodes) becomes less distorted, reflecting enhanced mechanical stability and coherence of motion.

Movie S3 (MPG)

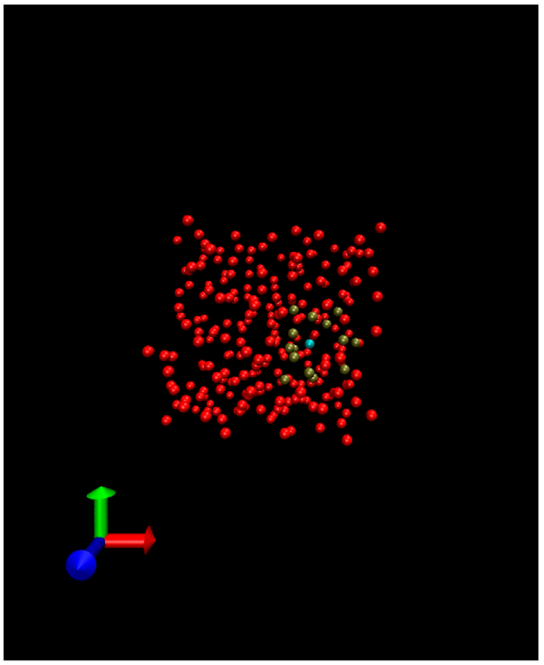

Movie S4 Nonmonotonic dependence of flow initiation and flow speed upon network connectivity. For Movies S3–S7, network connectivity varies with $P_c = 0.4$, 0.5, 0.6, 0.7, and 0.9, respectively. In all the cases, the whole lattice develops spontaneous directed motion and exhibits spatial modulation, indicating modulated flowing states. As P_c increases from 0.4 to 0.6 (Movies S3–S5), flow initiation accelerates and flow speed rises; as P_c further increases to 0.7 (Movie S6) and 0.9 (Movie S7), increasing the number of bond constraints appears to slow down flow initiation and to reduce flow speed. This suggests an optimal network connectivity (and thus optimal localization strength of the nodes) for most efficient flow. Meanwhile, as P_c increases, the nodes exhibit smaller amplitude of vibrations about the moving fiducial lattice and the cage of neighbors (as seen for the labeled nodes) becomes less distorted, reflecting enhanced mechanical stability and coherence of motion.

Movie S4 (MPG)

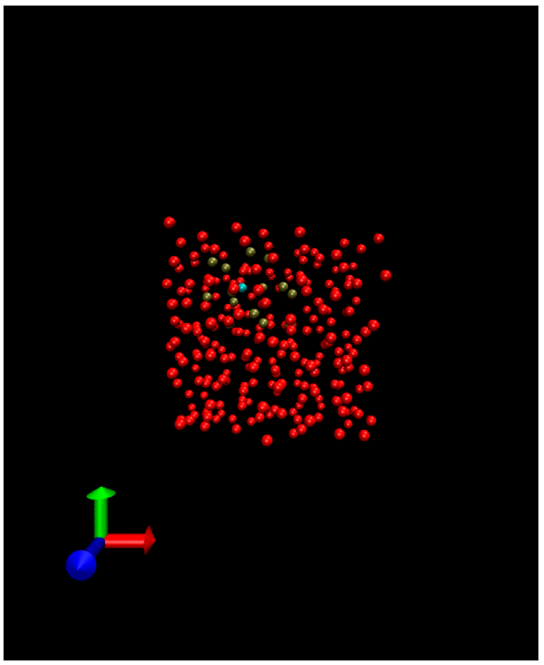

Movie S5 Nonmonotonic dependence of flow initiation and flow speed upon network connectivity. For Movies S3–S7, network connectivity varies with $P_c = 0.4$, 0.5, 0.6, 0.7, and 0.9, respectively. In all the cases, the whole lattice develops spontaneous directed motion and exhibits spatial modulation, indicating modulated flowing states. As P_c increases from 0.4 to 0.6 (Movies S3–S5), flow initiation accelerates and flow speed rises; as P_c further increases to 0.7 (Movie S6) and 0.9 (Movie S7), increasing the number of bond constraints appears to slow down flow initiation and to reduce flow speed. This suggests an optimal network connectivity (and thus optimal localization strength of the nodes) for most efficient flow. Meanwhile, as P_c increases, the nodes exhibit smaller amplitude of vibrations about the moving fiducial lattice and the cage of neighbors (as seen for the labeled nodes) becomes less distorted, reflecting enhanced mechanical stability and coherence of motion.

Movie S5 (MPG)

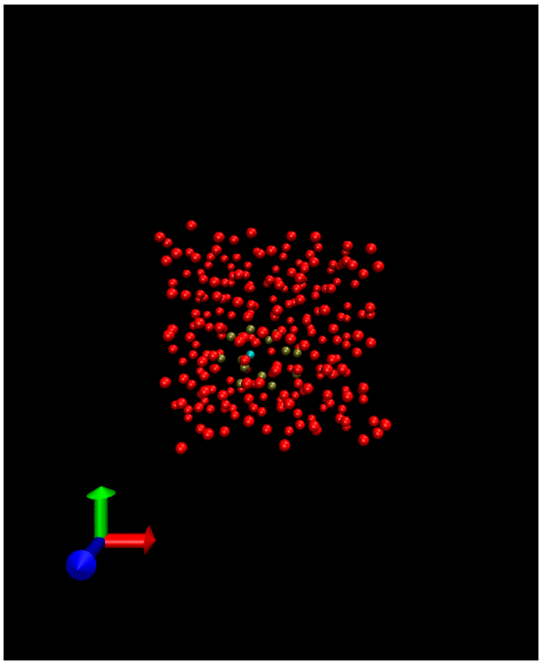

Movie S6 Nonmonotonic dependence of flow initiation and flow speed upon network connectivity. For Movies S3–S7, network connectivity varies with $P_c = 0.4$, 0.5, 0.6, 0.7, and 0.9, respectively. In all the cases, the whole lattice develops spontaneous directed motion and exhibits spatial modulation, indicating modulated flowing states. As P_c increases from 0.4 to 0.6 (Movies S3–S5), flow initiation accelerates and flow speed rises; as P_c further increases to 0.7 (Movie S6) and 0.9 (Movie S7), increasing the number of bond constraints appears to slow down flow initiation and to reduce flow speed. This suggests an optimal network connectivity (and thus optimal localization strength of the nodes) for most efficient flow. Meanwhile, as P_c increases, the nodes exhibit smaller amplitude of vibrations about the moving fiducial lattice and the cage of neighbors (as seen for the labeled nodes) becomes less distorted, reflecting enhanced mechanical stability and coherence of motion.

Movie S6 (MPG)

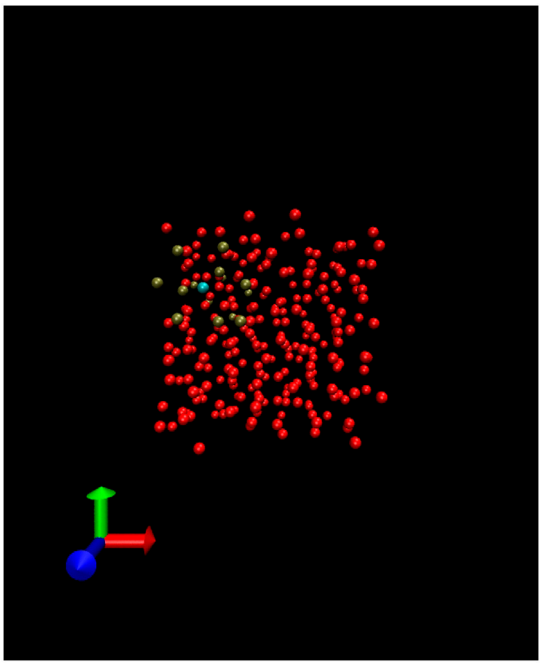

Movie S7 Nonmonotonic dependence of flow initiation and flow speed upon network connectivity. For Movies S3–S7, network connectivity varies with $P_c = 0.4$, 0.5, 0.6, 0.7, and 0.9, respectively. In all the cases, the whole lattice develops spontaneous directed motion and exhibits spatial modulation, indicating modulated flowing states. As P_c increases from 0.4 to 0.6 (Movies S3–S5), flow initiation accelerates and flow speed rises; as P_c further increases to 0.7 (Movie S6) and 0.9 (Movie S7), increasing the number of bond constraints appears to slow down flow initiation and to reduce flow speed. This suggests an optimal network connectivity (and thus optimal localization strength of the nodes) for most efficient flow. Meanwhile, as P_c increases, the nodes exhibit smaller amplitude of vibrations about the moving fiducial lattice and the cage of neighbors (as seen for the labeled nodes) becomes less distorted, reflecting enhanced mechanical stability and coherence of motion.

Movie S7 (MPG)